

RESEARCH ARTICLE

Open Access



Cdkn1a silencing restores myoblast differentiation by inducing selective apoptosis in senescent cells

Sujin Kim^{1,2†}, Bonsang Gu^{1,2,3†}, Chan-Young So^{1,2,3}, Keren Esther Kristina Mantik^{1,2,3}, Seung-Hyun Jung^{4,5,6}, Sohee Moon^{1,2}, Dong-Ho Park^{3,7}, Hyo-Bum Kwak^{3,7}, Jinkyung Cho⁸, Eun-Jeong Cho^{3,7}, Jae-Seon Lee^{2,3,9*} and Ju-Hee Kang^{1,2,3*} 

[†]Sujin Kim and Bonsang Gu contributed equally to this study.

*Correspondence: jaseslee@inha.ac.kr; johykang@inha.ac.kr

¹ Department of Pharmacology, Inha University College of Medicine, 100, Inha-Ro, Michuhol-Gu, Incheon 22212, Republic of Korea

⁹ Department of Molecular Medicine, Inha University College of Medicine, 100, Inha-Ro, Michuhol-Gu, Incheon 22212, Republic of Korea

Full list of author information is available at the end of the article

Abstract

Background: Sarcopenia, characterized by a progressive loss of skeletal muscle mass and function, is associated with the accumulation of senescent muscle stem cells, which impair muscle regeneration and contributes to the decline in muscle health. *Cdkn1a*, which encodes p21, is a well-known marker of cellular senescence. However, it remains unclear whether p21 inhibition eliminates senescent myoblasts and restores the differentiation capacity.

Methods: We performed transcriptomic analysis to identify genes related to aging-induced sarcopenia using 21 month-old Sprague–Dawley rats. To investigate the specific role of *Cdkn1a* gene in muscle aging, we used an in vitro model of ceramide-induced senescence in myoblasts, which was verified by the upregulation of p21 and increased senescence-associated beta-galactosidase (SA-β-gal) staining. To inhibit p21, we treated myoblasts with small interfering RNA (siRNA) targeting *Cdkn1a*. Using fluorescence-activated cell sorting, we separated subpopulations of cells with high or low caspase 3/7 activity. Protein expression related to myogenesis, muscle atrophy, protein synthesis, and apoptosis were quantified by western blotting.

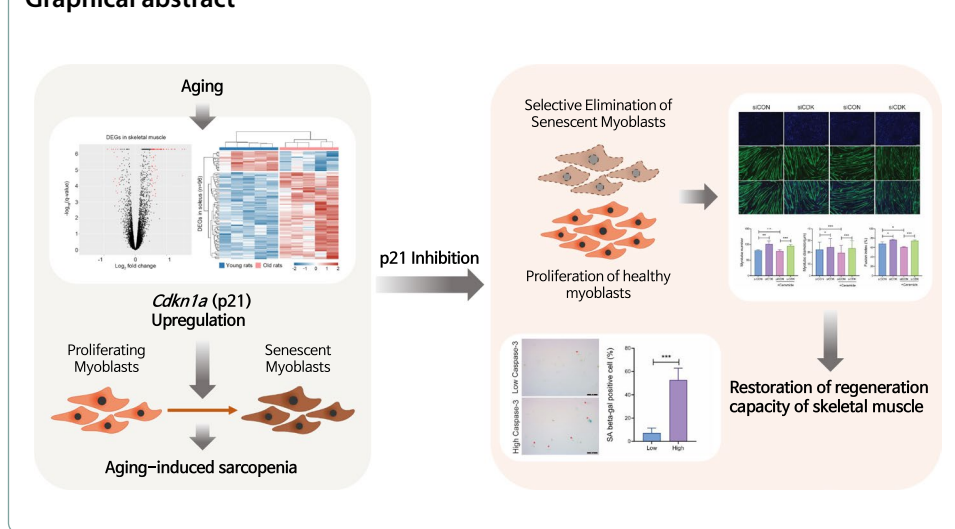
Results: In our transcriptomic analysis, we identified *Cdkn1a* as an upregulated gene in both the soleus and white gastrocnemius muscles of aged rats, among 36 commonly upregulated genes. The upregulation of *Cdkn1a* appears to be linked to mitochondrial dysfunction and cellular senescence, underscoring its significance in sarcopenia pathogenesis. C2-ceramide treatment effectively induced senescence, as evidenced by increased p21 expression, enhanced SA-β-gal staining, decreased myogenesis, and increased apoptosis. Knockdown of p21 in ceramide-treated myoblasts significantly reduced SA-β-gal-positive cells, restored cell proliferation, reduced the expression of senescence-associated cytokines (i.e., interleukin (IL)-6 and tumor necrosis factor (TNF)-α), and selectively induced apoptosis in the senescent cell population, demonstrating a senolytic effect. Notably, p21 inhibition also improved differentiation of myoblasts into myotubes, as indicated by increased myosin heavy chain expression and improvements in myotube diameter and fusion index.



Conclusions: Our data suggest that p21 inhibition selectively eliminates senescent cells while simultaneously enhancing the regenerative capacity of healthy myoblasts, which may combine to improve muscle regeneration and promote myogenesis, ultimately improving muscle health and function in aged individuals.

Keywords: p21, *Cdkn1a*, Senescence, Sarcopenia, Senolysis, Myogenesis

Graphical abstract



Background

Sarcopenia is a muscular disorder characterized by a progressive and generalized loss of skeletal muscle mass and strength [1]. Diagnostic markers for identifying severe sarcopenia are closely linked to reduced physical performance [2]. Although fundamental pathogenic mechanisms of primary sarcopenia—such as inflammatory processes, dysregulation of protein synthesis and degradation, neuromuscular degeneration, mitochondrial dysfunction, oxidative stress, and cellular senescence—have been proposed, the molecular mechanisms underlying sarcopenia remain incompletely understood [3–5]. Among these, the senescence of muscle stem cells (i.e., satellite cells) has been suggested as a key molecular mechanism driving sarcopenia [6]. Cellular senescence, which involves the loss of reversible quiescence, may impair the muscle’s regenerating capacity, as observed in elderly patients with sarcopenia.

P21, encoded by the *Cdkn1a* gene, influences a variety of cellular processes beyond cell cycle regulation, including DNA repair, apoptosis, senescence, and cell migration. In skeletal muscle, p21 plays a crucial role in myogenesis and differentiation, acting as a key determinant of whether myoblasts proliferate or differentiate [7–9]. Unlike other cell cycle regulators, p21 is co-expressed with myogenic transcription factors during the muscle differentiation process [10]. By interacting with the CDK4-cyclin D complex, p21 induces G1 phase cell cycle arrest, temporarily halting cell division during differentiation. This process allows muscle cells to grow and mature, with p21 being partially retained in mature skeletal muscle fibers [11]. Beyond its role in protecting differentiating cells from apoptosis, p21 also exerts anti-apoptotic effects by interacting with various apoptotic regulators [12, 13].

Previous studies suggest that p21 may be crucially involved in the onset mechanism of age-related sarcopenia [14, 15]. The accumulation of senescent cells, which are resistant to apoptosis, is a key factor promoting tissue dysfunction. In post-mitotic cells, such as skeletal muscle and neurons, chronic senescence activation may alter the microenvironment in a p21-dependent manner through paracrine intercellular communication [16]. Consistently, increased p21 expression in multinucleated myofibers is a common feature observed in the skeletal muscles of aged mice and elderly individuals [17, 18]. While p21 overexpression can lead to temporary cell cycle arrest that promotes muscle differentiation, it can also result in irreversible cell cycle arrest, a hallmark of cellular senescence [19]. Studies have shown that p21 overexpression in mice leads to increased expression of cell cycle regulatory factors, DNA damage markers, and inflammation-related factors. For example, the activation of the cellular senescence program in p21-overexpressing skeletal muscles is characterized by mitochondrial dysfunction, increased senescence-associated secretory phenotype (SASP) expression, reduced subcutaneous fat mass, decreased skeletal muscle weight, smaller cross-sectional area (CSA) of muscle fibers, and impaired physiological functions such as reduced running endurance and grip strength [14].

Taken together, p21 appears to play a significant role in the activation of senescence program in skeletal muscle. The association between p21 overexpression and skeletal muscle aging prompted us to investigate the effects of p21 inhibition on the reversal of myocyte senescence. In addition, treatment of aged mice with senolytic compounds (i.e., dasatinib + quercetin) has been shown to improve skeletal muscle mass and function while reducing the overexpression of p21 in aged skeletal muscle [20, 21]. However, it remains unclear whether inhibiting p21 alone can attenuate sarcopenia. To validate the upregulation of *Cdkn1a* in aged skeletal muscle, we performed transcriptomic analysis on both type I (soleus) and type II (white gastrocnemius) muscles from young and old rats, identifying the *Cdkn1a* gene as a potential therapeutic target for aging-related sarcopenia. Notably, we also observed senolytic effects following p21 inhibition in a myoblast model of senescence-associated sarcopenia.

Materials and methods

Animal care and experiments

All animal experiments performed were approved by the Institutional Animal Care and Use Committee of Inha University (IACUC approval number, INHA-180807-587-5, Incheon, Korea). We considered the median lifespan of Sprague–Dawley (SD) rats to ascertain a comparable age to elderly humans, and sacrificed old rats at the age of 21 months ($n=12$). We used 4-month SD rats old as young controls ($n=9$). Before sacrifice, rats were tested for grip strength to measure maximal forelimb strength. We collected cardiac blood for biochemical analysis, and isolated soleus and white gastrocnemius (WG) muscle to analyze the expression levels of mRNAs and proteins.

Skeletal muscle function test

Skeletal muscle strength was assessed by grip strength using an animal automated grip strength meter (Bioseb, Pinellas Park, FL, USA) 3 days before sacrifice. Briefly, rats were gently lifted by the tail and hung onto the grip bar by their front paws. When both

forepaws grasped onto the bar, the rats were gently pulled horizontally by the investigator until they released their grip. We calculated the maximal forelimb strength from the average of three best trials divided by the body weight. Muscle fatigue was assessed by calculating the fatigue index, which represents the decline in muscle strength over repeated measurements. Each animal underwent six consecutive trials to measure muscle strength. The fatigue index was calculated as the percentage decrease in performance, determined by comparing the average of the last two measurements (5th and 6th trials) with the average of the first two measurements (1st and 2nd trials). All muscle strength values were normalized to body weight to ensure consistency and comparability across samples.

Mitochondrial function test of skeletal muscle

Isolated skeletal muscles weighed approximately 2 mg and were permeabilized for mitochondrial function assays by incubation of myofiber bundles with sapoin (50 $\mu\text{g}/\text{mL}$). The permeabilized myofiber was washed with washing buffer (Buffer Z with 50 μM ethylene glycol-bis(β -aminoethyl ether)- $\text{N},\text{N},\text{N}',\text{N}'$ -tetraacetic acid [EGTA]) containing 105 mM K-MES, 30 mM KCl, 10 mM KH_2PO_4 , 5 mM $\text{MgCl}_2 \cdot 6\text{H}_2\text{O}$, and 0.5 mg/mL bovine serum albumin (BSA) (pH 7.1) for at least 15 min. The mitochondrial O_2 consumption rate was assessed using a polarographic high-resolution respirometer (O2K Oxygraph, Oroboros, Innsbruck, Austria) at 30 $^\circ\text{C}$ in an assay buffer (Buffer Z with 20 mM creatine and 50 μM EGTA), as previously described [22]. The substrate assessing O_2 flux was added sequentially as follows: (i) 5 mM glutamate + 2 mM malate (GM; complex I substrates); (ii) 4 mM ADP (state 3 condition); and (iii) 10 mM succinate. Mitochondrial O_2 respiration was expressed as pmol/sec/mg wet tissue weight. Mitochondrial H_2O_2 emission was measured in Buffer Z at 37 $^\circ\text{C}$ ($\Delta\text{F}/\text{min}$) during state 4 respiration (oligomycin, 10 $\mu\text{g}/\text{mL}$) by continuously monitoring the oxidation of Amplex Red (excitation/emission wavelengths $\lambda = 568/581$ nm) using a SPEX Fluormax 4 spectrofluorometer (HORIBA Jobin Yvon, Edison, NJ, USA). The substrates for H_2O_2 emission measurement were added sequentially as follows: (i) 5 mM glutamate + 2 mM malate (GM; complex I substrates); (ii) 10 mM succinate (complex II substrate); and (iii) 10 mM glycerol-3-phosphate (G3P; lipid substrate), as previously described [23]. The mitochondrial H_2O_2 emission rate following the deletion of values from each of the standard curves was measured from the slope of $\Delta\text{F}/\text{min}$ gradient values. The slope value was recalculated using a 10 point (total 30 s) overlapping moving average, and five consecutive ranges with the smallest slope variations were selected for analysis. All data were analyzed within the times between each substrate injection and the subsequent injection. The H_2O_2 emission was expressed as pmol/min/mg wet tissue weight. To summarize the mechanisms by which different substrates regulate mitochondrial O_2 respiration and H_2O_2 emission, GM supplies electrons to complex I, generating NADH, which drives electron transport through the electron transport chain (ETC) and enhances O_2 consumption. However, in terms of mitochondrial H_2O_2 emission, GM can lead to electron leakage at complex I and increased H_2O_2 generation. ADP stimulated ATP synthase activity, accelerating proton flux and increasing electron flow, while succinate provides FADH_2 , which directly supplies electrons to complex II, and further promotes O_2

reduction at complex IV. Succinate enhances O₂ consumption but also induces a reverse electron transport toward complex I, a major source of excessive H₂O₂, while G3P transfers electrons via G3P dehydrogenase, contributing to reactive oxygen species (ROS) generation through interactions with the ubiquinone pool.

The mitochondrial Ca²⁺ retention capacity was evaluated by monitoring changes in Ca²⁺-induced fluorescence ($\Delta F/\text{min}$) with the fluorescent dye, Calcium Green-5 N, at 37 °C under state 4 respiratory conditions. The assay buffer contained 1 μM Calcium Green-5 N, 5 mM glutamate, 2 mM malate, and 80 μM EGTA. Using a SPEX FluoroMax 4 spectrofluorometer (excitation/emission wavelengths = 506/532 nm), reactions were initiated by sequential addition of 30 μM Ca²⁺ pulses. The Ca²⁺ retention capacity was normalized to wet tissue weight for comparative analysis.

RNA extraction and whole transcriptome sequencing

Soleus muscles from five randomly selected young rats and five old rats, and WG muscles from four randomly selected young rats and three old rats, were subjected to transcriptomic analysis. Total RNA was purified using RNeasy kits (QIAGEN) following the manufacturer's protocol. RNA quantity and quality were measured using the Qubit (Thermo Fisher Scientific, Waltham, MA) and TapeStation (Agilent Technologies, Santa Clara, CA), respectively. For RNA sequencing, only total RNA sample with RNA integrity numbers ≥ 7 were used for analysis. Total RNA was then converted into a cDNA library using the TruSeq RNA Library Preparation Kit v2 (Illumina, San Diego, CA). After PCR amplification, the final product was assessed with a TapeStation (Agilent) and subsequently sequenced on the Illumina NovaSeq 6000 platform (Illumina) with 101-bp paired-end reads. Sequencing adapters and low-quality bases were trimmed using Trimmomatic software [24]. The trimmed sequencing reads were then mapped onto the *Rattus norvegicus* reference genome (Rnor_6.0, rn6) using the STAR aligner [25]. Gene-level quantification of expression was performed with HTSeq [26], according to the Ensembl transcript annotation (Rnor_6.0.91 version). Details of the whole transcriptome sequencing (WTS) data are available in Supplementary Table S4. Differentially expressed gene (DEG) analysis was performed using SARTools [27] and edgeR R packages [28]. DEGs were defined by adjusted *p*-values (false discovery rate) of < 0.001 and twofold log₂ fold change (i.e., log₂ fold change > 2 for upregulated and log₂ fold change < -2 for down-regulated genes). GO enrichment analysis was performed using Metascape [29]. The "biological process," "cellular components," "molecular function," and "KEGG pathways" categories were used in this analysis with default parameters (minimum overlap = 3, *p*-value cutoff = 0.01, minimum enrichment = 1.5).

Cell culture

C2C12 (ATCC, CRL1772, Manassas, VA, USA), mouse muscle cells were cultured in growth medium (GM) consisting of high glucose (25 mM) Dulbecco's modified Eagle's medium (DMEM; Gibco-Brl, Grand Island, NY, USA) supplemented with 10% fetal bovine serum (FBS; Gibco-BRL) and 1% penicillin–streptomycin (Gibco-BRL) at 37 °C with 5% CO₂ in a CO₂ incubator. When the cells reached approximately 70% confluency, they were passaged and used for experiments. Differentiation was stimulated using differentiation media (DM), consisting of DMEM with 2% horse serum (Gibco-BRL) and

1% penicillin–streptomycin (Gibco-BRL). The media were changed daily for 4 days to achieve complete myotube formation.

Chemical treatment and siRNA transfection

For the silencing of the *Cdkn1a* gene, siRNA transfection was conducted for 6 h, followed by a 16-h stabilization period in GM to allow the cells to recover from the exposure to the transfection mixture. The cells were then treated with GM containing C2-ceramide (50 μ M, d18:1/2:0, Avanti Polar Lipids, Alabama, USA) for 8 h, a condition that does not induce cytotoxicity [30, 31]. The siRNA transfection protocol followed the Bioneer siRNA user manual (AccuTarget Genome-wide Predesigned siRNA library). Three types of siRNA specific to *Cdkn1a* (Supplementary Table S5) were pooled. Lipofectamine RNAiMAX (Invitrogen, Carlsbad, California, USA) served as the transfection reagent. The siRNA and Lipofectamine RNAiMAX were separately added to Opti-Minimal Essential Medium (Opti-MEM; Gibco-BRL) optimized for transfection and allowed to incubate at room temperature (RT) for 5 min. Afterward, the mixture was incubated at RT for 20 min to form complexes before being applied to the cells. After 6 h, the transfection reagent was removed, and the media was replaced with GM for stabilization. The treatment concentration of siRNA-*Cdkn1a* and Lipofectamine RNAiMAX was 100 nM and 5 μ L/mL, respectively. The control group was treated with a negative control duplex siRNA (Bioneer, SN-1003).

Senescence-associated β -galactosidase (SA β -gal) staining

SA- β -gal staining of cells was performed using the Senescence Cells Histochemical Staining Kit (Sigma-Aldrich, Missouri, USA). Briefly, treated myoblasts were washed in phosphate buffered saline (PBS) and fixed for 6–7 min with a 1 \times fixation buffer. Cells were washed three times with PBS, and the staining mixture was added, followed by sealing with paraffin. The sealed plate was then stored in a CO₂-free incubator at 37 °C. The staining reaction was terminated at 16 h when the cells appeared blue–green, as visualized under an inverted microscope. Random images of three different locations on each slide were captured using a Leica DMIL LED microscope (Leica, Wetzlar, Germany) and the percentage of SA- β -gal-positive cells was calculated relative to the total number of cells.

Western blot

Cells were lysed with 200 μ L of radioimmunoprecipitation assay (RIPA) buffer (Elpis-Biotech, DaeJeon, Korea) that contained a 1% protease inhibitor cocktail (Sigma-Aldrich) and 10% Phos-Stop (Sigma-Aldrich). The cell lysate was scraped using a cell lifter, sonicated (Sonics & Materials sonicator; amplitude 20%, 5 s, 3 cycles) and centrifuged (16,000 \times g, 10 min, 4 °C) to obtain the protein extract. A protein amount of 13–20 μ g was loaded into each well and analyzed by SDS–polyacrylamide gel electrophoresis (SDS-PAGE). After SDS-PAGE, proteins were transferred to a nitrocellulose transfer membrane (NC; Pall corporation, Mexico). The membrane was incubated with 5% skimmed milk (Bio-Rad) in tris-buffered saline with Tween 20 (TBS-T) at RT for 2 h with shaking, and then incubated overnight at 4 °C with a specific primary antibody (Supplementary Table S6) in TBS-T containing 5% BSA (Sigma-Aldrich). Horseradish

peroxidase (HRP)-conjugated secondary antibodies (Invitrogen), either goat anti-mouse or goat anti-rabbit, diluted in 5% skimmed milk were allowed to incubate at RT for 2 h. The membrane was thoroughly reacted with Enhanced Chemiluminescence Detection reagent (ECL; Thermo Fisher Scientific). Protein bands were visualized using Chemidoc (Bio-Rad) equipment. The extracted protein bands were quantified using Image Lab software 6.0.1.

Quantitative reverse transcription PCR (qRT-PCR)

Cells were collected with Trizol reagent (Invitrogen) and the RNA was separated using chloroform, followed by precipitation with isopropanol. RNA quantity and purity were measured using the ND-1000 Spectrophotometer (NanoDrop Technologies, Wilmington, DE, USA). RNA, diluted to 1 µg, was used for cDNA synthesis using the Takara Bio cDNA synthesis kit according to the user guide. A thermocycler (Bio-Rad, Hercules, CA, USA) was used to amplify the specific gene using iQ™ SYBR® Green Supermix (Bio-rad). The sequences of primers for PCR are summarized in Supplementary Table S7.

Cell viability and propidium iodide (PI) staining assay

Treated cells underwent two washes with PBS, followed by trypsin–EDTA (Gibco-BRL) treatment at 37 °C with 5% CO₂ conditions in a CO₂ incubator for 2 min to facilitate cell separation. Cells were then collected using GM, mixed with 0.4% Trypan blue (Gibco-Brl) at a 1:1 ratio, and cell counting was performed using a hemocytometer. Cells detached using the same method as the cell viability assay were then collected using GM, followed by centrifugation (300 × *g*, 5 min). Cells were permeabilized at 4 °C for 30 min with 75% ethanol and stained with propidium iodide (PI) solution (50 µg/mL PI + 0.1 mg/mL RNase in PBS) for cell cycle analysis. Sample analysis was conducted using BD FACSCalibur™ Flow Cytometer (Becton, Dickinson and Company Biosciences, Franklin Lakes, USA), and data analysis utilized BD FlowJo v10 software.

Fluorescence-activated cell sorting (FACS) analysis

Cells, following ceramide treatment and gene knockdown, were subjected to the same washing and trypsin–EDTA treatment as described above. The detached cells were collected in GM and centrifuged at 300 × *g* for 5 min. After removing the supernatant, cells were resuspended and stained with Caspase-3/7 Detection Reagents (Invitrogen) in GM, followed by incubation at 37 °C for 30 min in the dark to ensure optimal staining. Flow cytometric analysis and sorting were performed using a BD FACS Melody™ Cell Sorter (Becton, Dickinson and Company Biosciences). Cells were excited with a 488 nm laser, and fluorescence from the Caspase-3/7 reagents was detected through a 530/30 band-pass filter. Cell populations exhibiting high caspase-3/7 activity were gated and sorted separately from the overall population. Post-sorting, cells were collected in GM and incubated at 37 °C with 5% CO₂ for 4 h to allow for recovery. These sorted cells were then used for subsequent downstream experiments, including SA-β-gal staining.

Immunofluorescence (IF)

Cells were fixed with 4% paraformaldehyde for 10 min after treatment. Following fixation, cells were permeabilized with 0.2% Triton X-100, washed twice with PBS, and

blocked with 5% BSA in PBS for 1 h. After blocking, the cells were incubated with the primary antibody (Supplementary Table S6) in 1% BSA overnight at 4 °C. The secondary antibody (anti-rabbit IgG [H + L], F(ab')₂ fragment [Alexa Fluor[®] 488 Conjugate, Invitrogen]) diluted in 1% BSA was added for 1 h at RT and kept in darkness. Cells were washed twice with PBS and mounted on slides using mounting medium with 4',6-diamidino-2-phenylindole (DAPI; Vector, Newark, CA, USA). The primary antibody was diluted 1:200, and the secondary antibody was diluted 1:500.

Myotube morphology analysis

Analysis of myotube diameter, number, and fusion index was conducted using immunofluorescence microscopy with antibodies targeting myosin heavy chain (MHC) and DAPI. Myotubes were defined as cells with three or more nuclei within the tube structure to exclude myoblasts undergoing similar division. Random images from three different locations on each slide were captured using an Olympus IX83. Image analysis was conducted using ImageJ (Java) software. The fusion index was calculated as the percentage of nuclei number in each myotube with two or more nuclei relative to the total number of nuclei.

TUNEL assay

To assess DNA fragmentation, a TUNEL assay was performed using the Click-iT[™] TUNEL Alexa Fluor[™] 488 Imaging Assay Kit (Invitrogen, A23210). C2C12 myoblasts were first transfected with *Cdkn1a* siRNA, treated with ceramide for 8 h, and sorted on the basis of caspase-3/7 activity (high versus low). Sorted cells were then seeded in a 6-well plate at a density of 3×10^5 cells/well. Cells were fixed with 1% paraformaldehyde (PFA) on ice for 15 min and washed with Wash Buffer B. DNA labeling was performed by adding DNA Labeling Solution, prepared by mixing Reaction Buffer, TdT enzyme, BrdUTP, and H₂O, followed by incubation at 37 °C for 1 h. After labeling, cells were rinsed twice with Rinse Buffer and incubated with Alexa Fluor[®] 488 BrdU antibody solution at room temperature for 30 min. Finally, cells were treated with RI/RNase Buffer, and fluorescence intensity was measured to evaluate DNA fragmentation.

BrdU assay

C2C12 myoblasts were seeded in a 96-well plate (1×10^3 cells/well) and transfected with siRNA for 6 h, followed by ceramide treatment for up to 8 h. Cell proliferation was assessed in a time-course manner using the Cell Proliferation ELISA, BrdU (colorimetric) kit (Roche, 11647229001). BrdU labeling solution (10 μM) was added (10 μL/well) and incubated for 2 h. After fixation and DNA denaturation with FixDenat solution (200 μL/well, 30 min, RT), Anti-BrdU-POD working solution (100 μL/well) was added and incubated for 90 min at RT. Wells were washed, and the substrate solution (100 μL) was added for color development (10 min, RT). Absorbance was measured at 450 nm.

Statistical analysis

Data are presented as mean ± standard deviation (SD). Statistical analysis was conducted using GraphPad Prism Software Version 10.1.0. Unpaired *t*-tests or Mann–Whitney tests were used to determine significance between two groups. The protein densitometry,

relative mRNA expression, relative fluorescence intensity, and cell viability in response to ceramide treatment and siRNA transfection were analyzed using one sample *t*-tests. When comparing with untreated control, *p*-values < 0.05 were considered statistically significant.

Results

Characteristics of skeletal muscle and blood biochemistry in old rats

The weight of the soleus and WG muscles in old rats were significantly lower than those in young rats. The mean maximal forelimb strength of young rats was 1.7-fold higher than that of old rats, and the fatigue index in forelimb strength was significantly lower in young rats compared with old rats (Table 1). The levels of insulin, lipids, alanine aminotransferase (ALT), and aspartate aminotransferase (AST) are provided in Supplementary Table S1. The levels of AST, total cholesterol, LDL, and triglycerides were significantly higher in old rats than in young rats, while insulin, ALT, free fatty acids, and HDL were comparable between the two groups. Mitochondrial dysfunction is a feature of senescent tissue and sarcopenia [32] that results in elevated oxidative stress and diminished ATP production, ultimately contributing to a decline in muscle performance with aging. Therefore, we measured the mitochondrial O₂ respiration rate, H₂O₂ emission and calcium retention capacity to measure mitochondrial function in the soleus and WG muscles from each rat (Fig. 1). In aged skeletal muscle, both type I and type II muscle exhibited distinct alterations in mitochondrial O₂ consumption and H₂O₂ emission, depending on the substrate utilized. O₂ consumption was significantly reduced in the old group across GM, ADP, and succinate conditions, indicating a functional decline in complex I and II-driven respiration and ATP synthase activity. These results suggest age-related impairments in electron transport chain (ETC) efficiency, reflecting compromised mitochondrial function in muscle. In contrast, H₂O₂ production was elevated in the old group with GM, succinate, and G3P. The increase in H₂O₂ with GM and succinate suggests enhanced electron leakage from complex I and II, while elevated H₂O₂ with G3P implies greater ROS generation via the G3P shuttle. This heightened oxidative stress likely contributes to impaired muscle function. Ca²⁺ retention capacity, a crucial indicator of mitochondrial function in aging-related sarcopenia, was significantly decreased in both muscle types in the aged group compared with the young group. This reduction in Ca²⁺ retention capacity indicates premature opening of the mitochondrial permeability transition pore [33], which is consistent with typical mitochondrial dysfunction observed in aging muscle. Collectively, these findings demonstrate that old rats have a sarcopenic phenotype by mitochondrial dysfunction.

Table 1 Comparison of skeletal muscle mass and function in old and young rats

Variables	Young	Old	<i>p</i> -Value
Body weight (g)	477.40 ± 35.80	757.32 ± 91.44	< 0.001
Soleus/body weight (g/g)	0.38 ± 0.03	0.46 ± 0.04	< 0.001
Gastrocnemius/body weight (g/g)	4.56 ± 0.38	3.24 ± 0.31	< 0.001
Maximal forelimb strength (g/body weight)	2.40 ± 0.45	1.40 ± 0.30	< 0.001
Fatigue index (%)	10.90 ± 2.45	35.81 ± 6.74	0.007

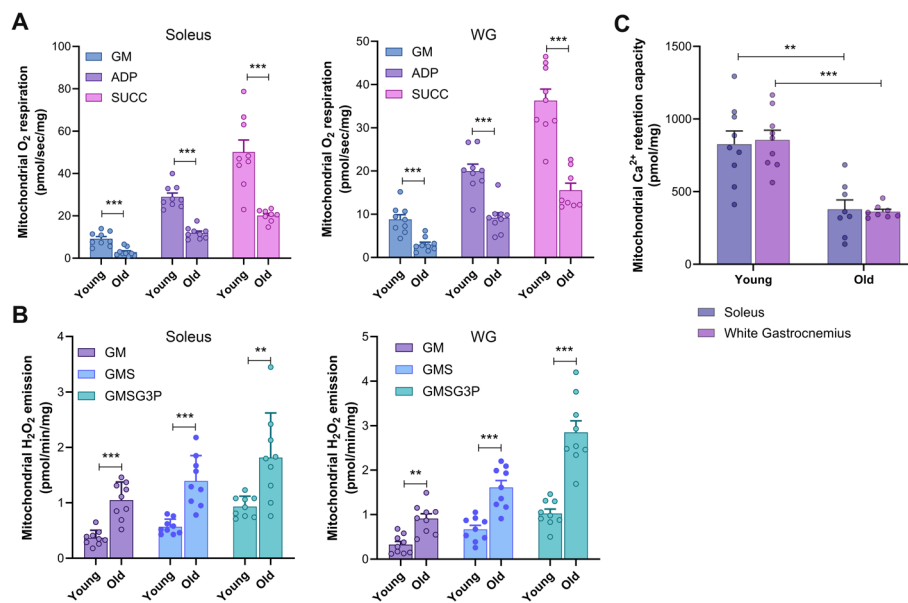


Fig. 1 Mitochondrial function in the skeletal muscles of young and old rats. **A** Mitochondrial O_2 respiration in the (left) soleus and (right) white gastrocnemius muscle (WG, $n=9$). **B** Mitochondrial H_2O_2 emission rate in the (left) soleus and (right) white gastrocnemius muscle (WG, $n=9$). **C** Mitochondrial calcium retention capacity in the soleus and white gastrocnemius muscle ($n=9$). ** $p < 0.01$, *** $p < 0.001$ by unpaired t -test. GM, glutamate + malate; ADP, adenosine diphosphate; Succ, succinate; GMS, GM + succinate; GMSG3P, GMS + glycerol 3 phosphate

Differentially expressed genes in old rats

We performed DEG analysis between the young and old rat groups, identifying 96 genes (78 upregulated and 18 downregulated; Fig. 2A left) and 206 genes (186 upregulated and 20 downregulated; Fig. 2B left) in the soleus and WG, respectively, as aging-related DEGs (Supplementary Table S2). In the unsupervised hierarchical clustering analyses of the DEGs, both the soleus and WG muscles revealed a complete separation between the young and old rat groups (Fig. 2 middle). The signatures of “positive regulation of cell activation,” “lymphocyte mediated immunity,” and “immune effector process” were enriched in aged rats, whereas those of “osteoblast differentiation” and “cytoskeleton in muscle cells” were enriched in young rats (Fig. 2 right; Supplementary Table S3).

Among the DEGs, 36 upregulated and 3 downregulated genes were commonly altered in both the soleus and WG (Fig. 2C). We further selected the *Cdkn1a* gene for downstream analysis based on its significance level, fold change, and relevance to aging-related sarcopenia pathogenesis [8–10]. Aging prominently accelerates the decline of type II muscle fibers, such as tibialis anterior and WG muscle, resulting in a pronounced fast-to-slow fiber type shift [34]. Notably, the expression level of *Cdkn1a* in aged rats was 4.5 times higher in the soleus (adjusted $p=7.4 \times 10^{-13}$) and 14.5 times higher in the WG (adjusted $p=6.0 \times 10^{-19}$) compared with that in young rats (Supplementary Table S2). In addition to *Cdkn1a*, commonly upregulated genes in both soleus and WG muscle include *Runx1*, *Gadd45a*, *Ankd1*, *Rrad* and *TMEM158*, which were also upregulated in the skeletal muscles of aged mice and responded to senolytics (Fig. 2C) [21].

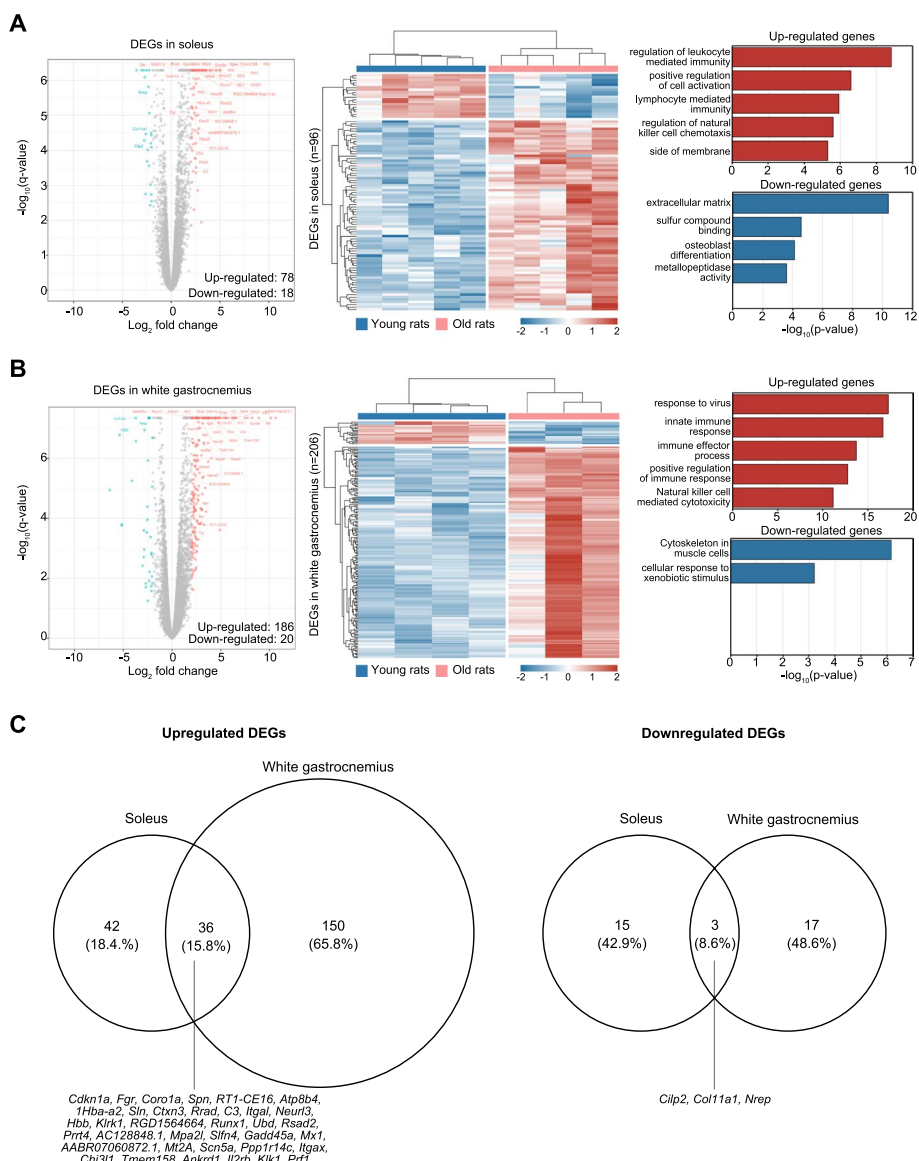


Fig. 2 Transcriptomic analysis of the skeletal muscles of young and old rats. **A, B** (Left) Volcano plots depicting differentially expressed genes (DEG) in the soleus (**A**) and white gastrocnemius (**B**) muscles. Red and blue dots indicate significantly upregulated and downregulated genes (adjusted $p < 0.001$) with a \log_2 fold change > 2 or < 2 , respectively. (Middle) Heatmap of DEGs between skeletal muscles of young and old rats. (Right) Gene Set Enrichment Analysis (GSEA) of enriched pathways between young versus old rats. **C** Numbers inside the circles indicate the count of upregulated and downregulated genes in the white gastrocnemius and soleus muscles. Commonly upregulated and downregulated genes in both muscles are listed

C2-ceramide induces senescence and mechanisms related to sarcopenia in C2C12 myoblasts

On the basis of previous studies showing that ceramide promotes cellular senescence, we treated C2C12 myoblasts with C2-ceramide to assess its potential to induce cellular senescence [30, 31]. To evaluate C2C12 myoblasts treated with C2-ceramide as a model for age-related sarcopenia, we examined the levels of SA- β -Gal staining, expression of

senescence-related proteins, and the mRNA expression levels of inflammatory factors. After treatment with 50 μM C2-ceramide for 8 h, the number of cells positively stained for SA-β-Gal (a cellular senescence marker) significantly increased (Fig. 3A, B). Moreover, the expression level of the p21 protein, another marker of cellular senescence, was significantly increased by ceramide treatment. However, there was no significant difference in the protein expression levels of p53 and p16, which are also markers of cellular senescence, suggesting that p21 upregulation may occur independently of p53 (Fig. 3C–F). In addition, ceramide increased the mRNA expression levels of other senescence-associated markers (Fig. 3G).

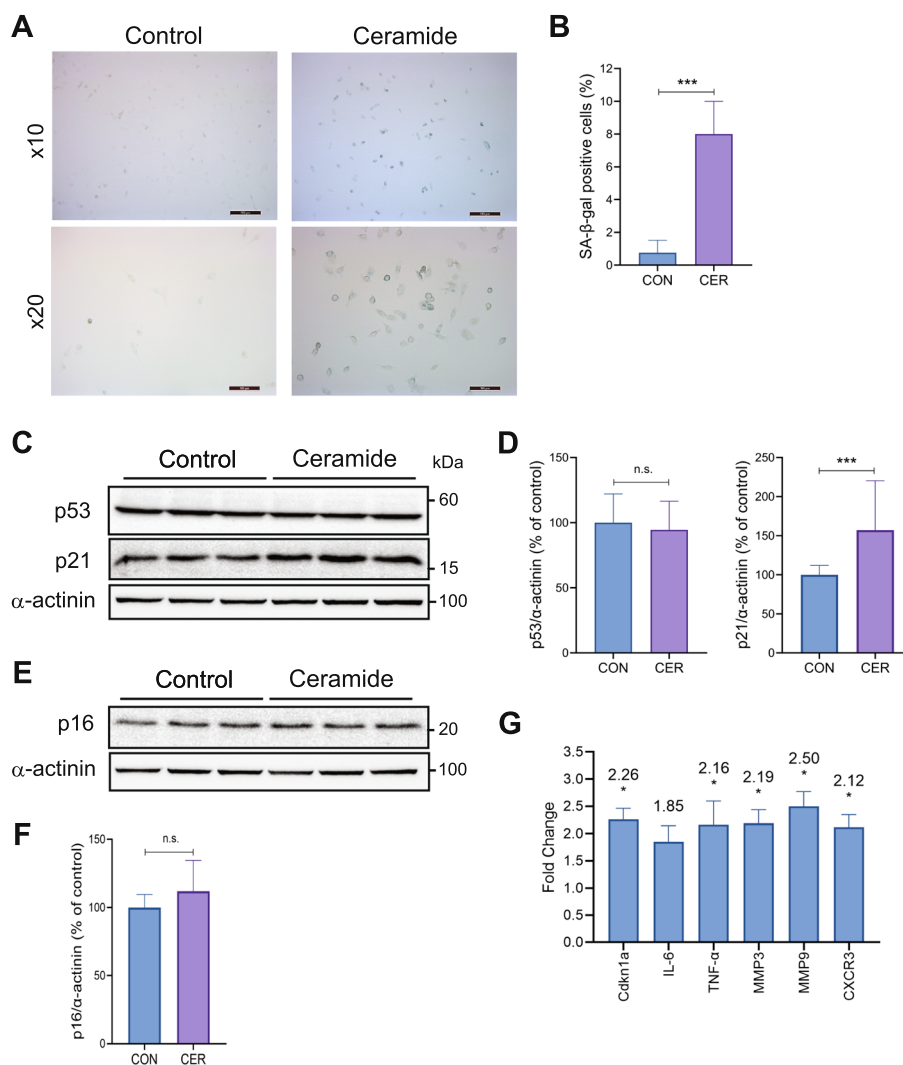


Fig. 3 Ceramide-induced senescence in myoblasts. **A, B** SA-β-gal staining of myoblasts. Cells with a blue stain indicate a senescent myoblast. **B** The number of senescent cells in ceramide-treated myoblasts was significantly higher than in vehicle controls ($n=9$). **C–F** Ceramide significantly upregulated the expression of p21 protein ($n=17$), while levels of p53 and p16 remained comparable ($n=6$). **G** mRNA levels of senescence markers in ceramide-treated myoblasts were higher than those in vehicle controls ($n=3$). The numbers in the graph indicate the fold changes relative to the control. ** $p < 0.01$, *** $p < 0.001$ by unpaired t -test. CER, ceramide; IL-6, interleukin-6; TNF-α, tumor necrosis factor-α; MMP-3, matrix metalloproteinase-3; MMP-9, matrix metalloproteinase-9; CXCR3, C-X-C Motif chemokine receptor 3

Next, we examined the expression levels of proteins involved in muscle atrophy, protein synthesis, and apoptosis. Ceramide treatment significantly decreased the level of phosphorylation of Akt and FOXO3a, which was linked to the upregulation of muscle atrophy-related protein MAFbx and the inhibition of the mTORC1-mediated protein synthesis pathway (Fig. 4A, B). Protein synthesis and translation processes are critical to myogenesis and muscle growth [35, 36]. Ceramide treatment reduced the phosphorylation levels of proteins regulating protein synthesis and translation, 4EBP1 and P70S6K. Furthermore, the expression of the key myogenesis factor MyoD was significantly lower in ceramide-treated cells compared with controls (Fig. 4A, B). While the pro-apoptosis protein Bax showed no significant changes, the anti-apoptotic protein Bcl-2 significantly decreased with ceramide treatment. In addition, ceramide treatment significantly increased the levels of representative markers of apoptosis, cleaved caspase-3 and cleaved poly ADP-ribose polymerase (PARP) (Fig. 4C, D). Combined, C2-ceramide-treated C2C12 myoblasts exhibited activation of underlying mechanisms of age-related sarcopenia.

p21 knockdown selectively enhances apoptosis in ceramide-induced senescent myoblasts

To investigate the role of p21 in the age-related sarcopenia model, we knocked down p21 and examined the changes in cellular senescence and sarcopenia-related factors.

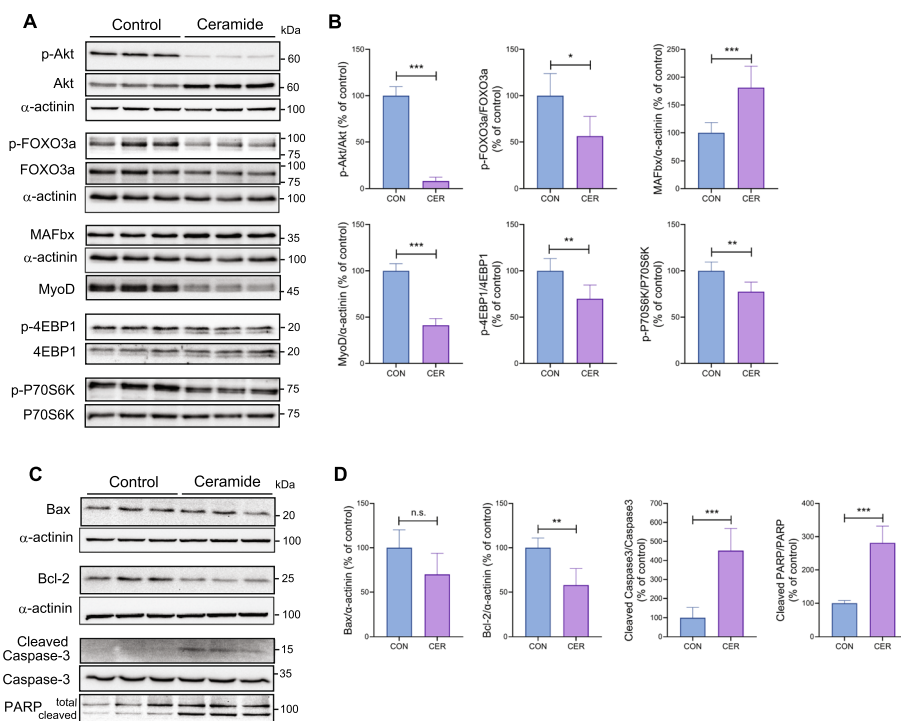


Fig. 4 Effects of ceramide on proteins involved in myogenesis, protein synthesis, muscle atrophy, and apoptosis. **A, B** Ceramide significantly downregulated the levels of MyoD, phosphorylated 4EBP1 and P70S6K (protein synthesis pathway), and phosphorylated Akt-FOXO3a. Ceramide upregulated the expression of the atrophy-related E3 ligase MAFbx, a downstream target of the Akt-FOXO3a pathway. **C, D** Ceramide increased the levels of apoptosis-related proteins. * $p < 0.05$, ** $p < 0.01$, *** $p < 0.001$ by unpaired t -test. CER, ceramide; FOXO3a, forkhead box O3 alpha; MAFbx, F-box only protein 32; PARP, poly ADP-ribose polymerase

When we treated myoblasts with siRNA, the efficiency of siCDK (estimated from triplicate experiments) was 64%. The increase in SA-β-Gal staining induced by C2-ceramide in myoblasts was significantly restored by p21 knockdown (Fig. 5A, B). However, the expression levels of p53 and p16 showed no significant changes (Fig. 5C, D). The phosphorylation levels of Akt and FOXO3a, as well as the expression of MAFbx and MyoD were not significantly recovered by p21 knockdown. (Fig. 5E, F). In addition, phosphorylation of proteins related to protein synthesis, namely 4EBP1 and P70S6K, did not show significant differences following p21 knockdown (Fig. 5G). Among proteins involved in apoptosis, Bax showed no significant difference, while Bcl-2 exhibited a significant decrease. Interestingly, the levels of cleavage of caspase-3 and PARP, which were increased by ceramide treatment, were further increased by p21 knockdown (Fig. 5E, F).

Next, we measured cell viability and the cell cycle to elucidate the effects of p21 silencing on cell death and proliferation in a subpopulation of cells. Interestingly, p21 knockdown led to a notable restoration of the ceramide-induced decrease in cell viability (Fig. 6A). To confirm that the increased cell survival due to p21 knockdown was attributed to enhanced proliferation through the inhibition of cell cycle arrest, we conducted cell cycle analysis using flow cytometry. C2-ceramide treatment increased the number of cells in G0/G1 and G2/M phases while decreasing in the number of cells in the S phase. Moreover, it was observed that the G1 cell cycle arrest induced by ceramide was inhibited by p21 knockdown (Fig. 6B). The hypothesis that the increased expression of apoptotic signals following p21 silencing (Fig. 5) arose from a subpopulation of ceramide-induced senescent cells was tested by analyzing apoptosis using FACS. In ceramide-treated cells, elevated caspase-3/7 activity was observed in a subset of cells,

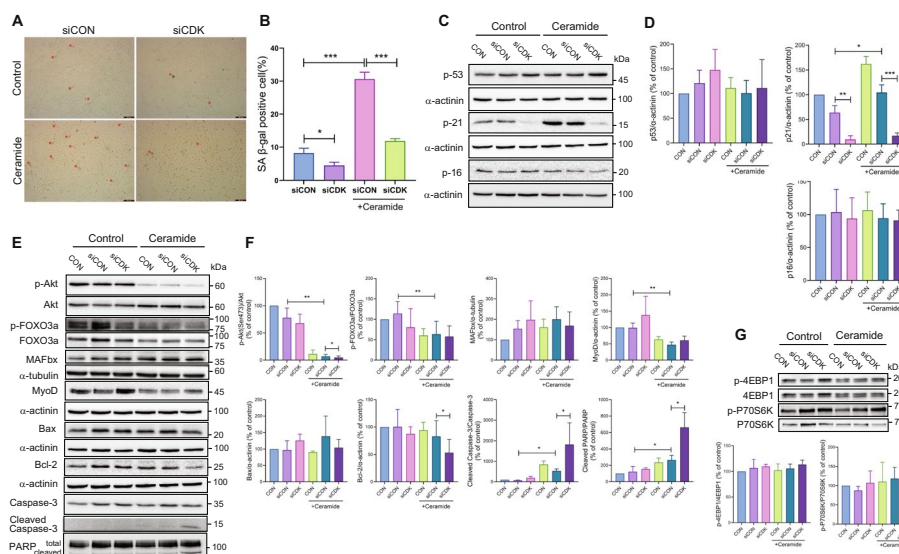


Fig. 5 Effects of *Cdkn1a* silencing on ceramide-induced myoblast senescence and cell death. **A, B** *Cdkn1a* silencing significantly inhibited ceramide-induced myoblast senescence ($n = 3$). Asterisks indicate senescent myoblasts. **C, D** siRNA treatment dramatically inhibited the expression of p21, but not p53 or p16 expression ($n = 3$). **E, F** *Cdkn1a* silencing had no significant effect on the levels of proteins involved in myogenesis or muscle atrophy. However, *Cdkn1a* silencing significantly augmented ceramide-induced upregulation of apoptosis-related proteins, including cleaved caspase-3 and cleaved PARP ($n = 3-5$). **G** *Cdkn1a* silencing had no significant effect on the expression of protein synthesis pathways ($n = 3-4$). * $p < 0.05$, ** $p < 0.01$, *** $p < 0.001$ by unpaired t-test

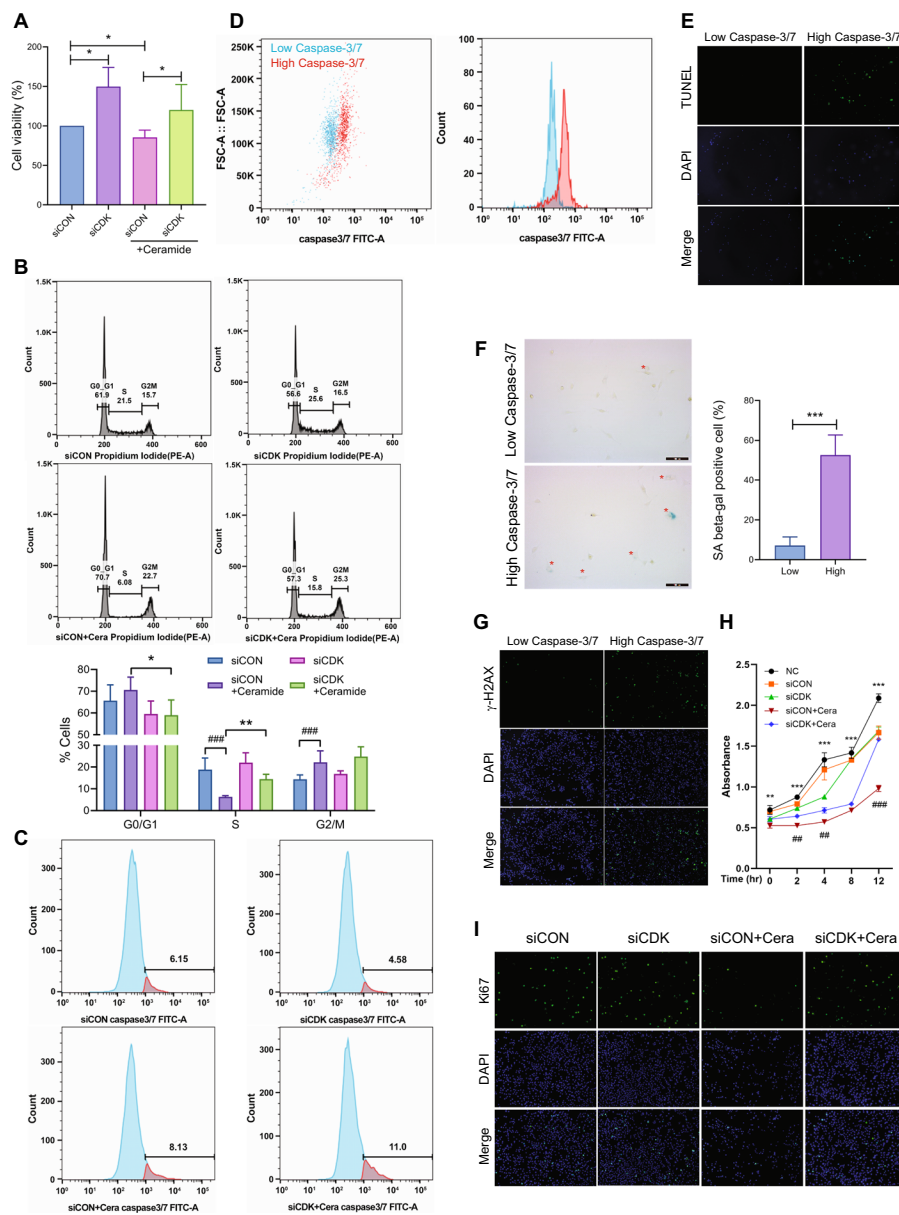


Fig. 6 Effects of ceramide and p21 knockdown on the cell cycle and survival of senescent myoblasts. **A** *Cdkn1a* silencing significantly increased the viability of ceramide-treated myoblasts ($n=5$). **B** Cell cycle analysis showed that ceramide-induced G1 cell cycle arrest was attenuated by *Cdkn1a* silencing ($n=5$). $*p < 0.05$, $**p < 0.01$, $###p < 0.001$ by unpaired *t*-test. **C** FACS analysis based on caspase-3/7 activity following ceramide treatment, with or without *Cdkn1a* silencing, confirmed increased caspase-3/7 activity with *Cdkn1a* knockdown. **D** Cell sorting based on caspase-3/7 activity following ceramide treatment and *Cdkn1a* silencing showed results consistent with **(E)** TUNEL staining ($n=3$). Compared with cells with low caspase-3/7 activity, cells with high caspase-3/7 activity exhibited a greater number of **(F)** SA- β -gal-positive cells ($n=11$) and **(G)** γ H2AX-positive senescent cells ($n=3$). Representative images acquired using a microscope at 10 \times magnification are shown. **F** Asterisks indicate senescent myoblasts. $*p < 0.05$, $***p < 0.001$ by unpaired *t*-test. **H** BrdU assay shows that siCDK restores the proliferation capacity of ceramide-treated myoblasts ($n=6$ per group). Vertical bars indicate standard errors. Two-way analysis of variance (ANOVA) revealed a significant time \times group interaction ($F=10.88$, $p < 0.001$). $**p < 0.01$, $***p < 0.001$ (siCON versus siCON + ceramide group [siCON + Cera]); $##p < 0.01$, $###p < 0.001$ (siCON + Cera versus siCDK + ceramide [siCDK + Cera]) by unpaired *t*-test. **I** Ki67 staining revealed that ceramide treatment inhibits the cell cycle, which is restored by *Cdkn1a* silencing ($n=3$). Representative images acquired using a microscope at 10 \times magnification are shown. Representative images from triplicate experiments are shown. γ H2AX, H2A histone family member X; Ki67, antigen Kiel 67; DAPI, 4',6-diamidino-2-phenylindole

and the number of these cells was further increased with p21 knockdown (Fig. 6C). Cell sorting was conducted on the basis of caspase-3/7 activity, dividing cells into the top 10% and bottom 10%, and the sorted cells were analyzed to validate the results (Fig. 6D). Cells with high caspase-3/7 activity exhibited increased apoptosis in the TUNEL assay compared with those in the low activity group (Fig. 6E). SA- β -Gal staining of the sorted cells showed that caspase-3/7 high (top 10%) cells were approximately 7.38 times more highly stained than caspase-3/7 low (bottom 10%) cells (Fig. 6F). This finding was further supported by increased γ H2AX staining, another senescence marker, in cells with high caspase-3/7 activity (Fig. 6G). To further validate the recovery effect of p21 knockdown, we performed a BrdU assay for 12 h, corresponding to the doubling time of C2C12 myoblasts. Compared with the siCON + ceramide group, the siCDK + ceramide group exhibited a higher proliferative capacity (Fig. 6H). In addition, we evaluated Ki67 as another marker to better understand the roles of p21 in cell cycle regulation. Our findings showed that ceramide treatment reduced the number of Ki67-positive cells, whereas p21 knockdown in ceramide-treated cells reversed this effect (Fig. 6I). These data suggest that p21 inhibition may facilitate the selective removal of senescent cells while supporting the proliferation of non-senescent cells.

p21 knockdown restores ceramide-induced inhibition of myogenesis

We investigated the effect of p21 knockdown on myogenesis in differentiated myotubes in an age-related sarcopenia model. We observed a decrease in both fast-twitch and slow-twitch isoforms of MHC (MHC[F] and MHC[S]), proteins related to muscle contraction, in the ceramide-treated group. Notably, a significant recovery was observed in MHC[S] following p21 knockdown, while no recovery was noted in MHC[F]. In addition, myogenin and myoD, showed no significant differences (Fig. 7A, B). To assess the maturation status of fully differentiated myotubes, we performed quantitative analysis of the diameter, number, and fusion index after fluorescent staining of MHC. The diameter and fusion index of myotubes modestly but significantly decreased following C2-ceramide treatment, and p21 knockdown led to a significant recovery. Although the number of myotubes and the mitochondrial O₂ respiration rate (Supplementary Information, Fig. S1) did not significantly decrease with C2-ceramide treatment, p21 knockdown resulted in a significant increase (Fig. 7C, D). We evaluated the effect of p21 knockdown on myotube differentiation and observed no significant impact (Supplementary Information, Fig. S2). Concurrently, ceramide induced the mRNA expression of IL-6 and TNF- α , well-known SASP cytokines in sarcopenia [37], which were significantly attenuated by p21 knockdown (Fig. 7E). These data suggest that the increased proliferation and senolysis induced by p21 knockdown might enhance differentiation into myotubes, particularly evident in the restoration of MHC[S] expression and the attenuation of upregulation of SASP cytokines.

Discussion

This study explored the potential of p21 inhibition to restore myoblast differentiation by selectively inducing apoptosis in senescent cells, a key contributor to sarcopenia [6]. During myoblast differentiation, p21 contributes to the shift from proliferation to differentiation by inhibiting the cell cycle [8, 9], in addition to inducing senescence

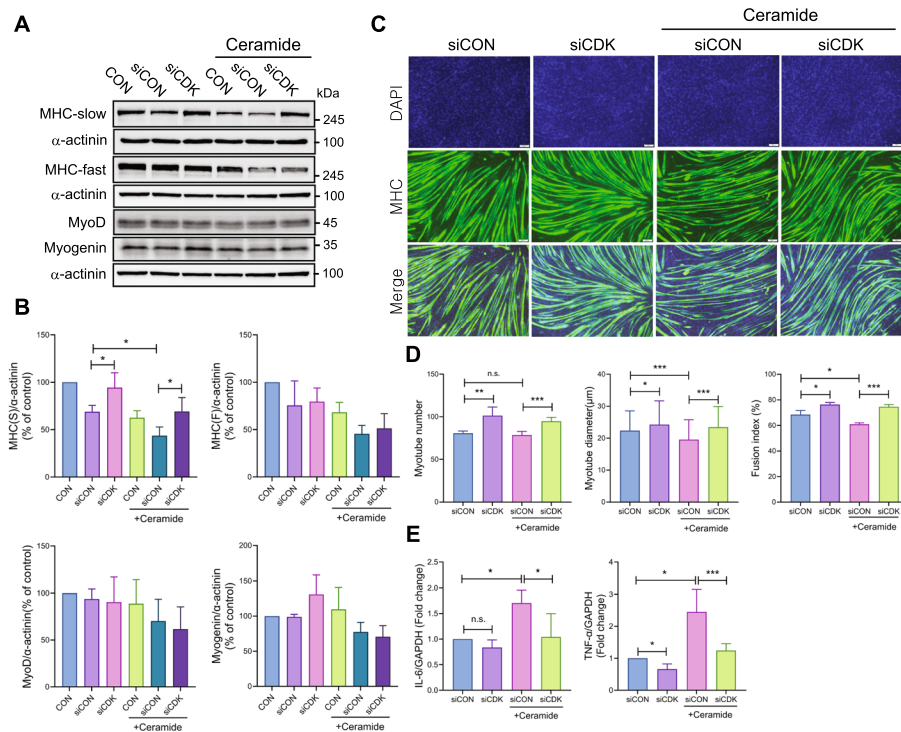


Fig. 7 p21 knockdown restores differentiation capacity in ceramide-treated myoblasts. **A, B** *Cdkn1a* silencing significantly restored the ceramide-induced downregulation of MHC (type I; slow) expression ($n = 3$). **C, D** The ceramide-induced inhibition of myocyte differentiation was significantly restored by *Cdkn1a* silencing ($n = 5$). **E** *Cdkn1a* knockdown significantly inhibited the ceramide-induced upregulation of senescence-associated secretory cytokines, IL-6 and TNF- α ($n = 4$). * $p < 0.05$, ** $p < 0.01$, *** $p < 0.001$ by unpaired *t*-test. MHC, myosin heavy chain; IL-6, interleukin-6; TNF- α , tumor necrosis factor-alpha

by aging stimuli. In our experimental conditions, ceramide induces p21 expression and cellular senescence in myoblasts, which is associated with decreased myotube differentiation and fusion. Therefore, our findings suggest that the role of p21 may be context-dependent based on the type of stimulation.

In aged rats, *Cdkn1a* expression was elevated in both soleus (type I) and WG (type II) muscles, correlating with mitochondrial dysfunction, oxidative stress, and reduced muscle mass and function, in agreement with previous studies linking p21 overexpression to age-related skeletal muscle dysfunction [14]. High p21-expressing myofibers in aged mice also exhibited senescence hallmarks, including activation of immune pathways [17]. Consistently, our GSEA similarly showed enrichment in immune responses (Fig. 2), and several upregulated genes matched with a previous report (Supplementary Fig. S1; Supplementary Table S2) [17]. Despite increased *Cdkn1a* expression being well-documented in aging muscle [15, 17], it remains unclear if manipulating *Cdkn1a* expression can mitigate sarcopenia and the mechanisms involved [38]. In C2-ceramide-treated myoblasts, p21 expression was upregulated alongside increased apoptotic markers and senescence markers, supporting its involvement in senescence and aging-induced sarcopenia [39]. When p21 was knocked down by silencing *Cdkn1a* in ceramide-treated myoblasts, the inhibition of myotube differentiation was recovered, although the decreased expression

of myogenic proteins (p-Akt/p-FOXO and MyoD) was not significantly restored. Notably, p21 knockdown reversed the senescence markers (i.e., IL-6 and TNF- α) and selectively triggered apoptosis in senescent cells, while preserving proliferating cells, indicating a senolytic effect. Consistent with a previous study [31], our observation showed ceramide-induced G1 arrest and an increased number of senescent cells, aligning with reports on the role of p21 in promoting senescence and muscle dysfunction [14]. We observed that p21 knockdown enabled myoblasts to overcome G1 arrest, enhancing their regenerative capacity through increased proliferation and cell cycle re-entry. Taken together, these results suggest that p21 inhibition may aid in clearing senescent cells and supporting muscle regeneration but has no significant effect on the p-Akt/p-FOXO pathway or MyoD expression.

Notably, p21 knockdown also restored myotube differentiation, with *Cdkn1a* silencing improving myogenic differentiation without impairing myotube formation. We observed enhanced slow-twitch MHC isoform expression, myotube diameter, and fusion index under p21 knockdown, suggesting a role in muscle regeneration by enhancing myoblast differentiation. This is consistent with prior research highlighting the role of p21 in muscle differentiation [7, 8], and suggests that its inhibition may reverse aspects of cellular senescence in sarcopenia. Previous studies also showed that p21 knockdown in the tibialis anterior muscle enhanced proliferation, muscle CSA, strength, and fatigue resistance [40], with miR-208b similarly targeting p21 to promote myoblast proliferation by reducing G1-phase cells and favoring a slow fiber phenotype with improved endurance [41, 42]. Our findings suggest that p21 reduction not only improves cell proliferation but also reverses senescence, contributing to muscle health.

Senescent cells accumulate in various tissues with age, releasing SASP that contribute to tissue dysfunction [43]. Clearing these cells can alleviate pathologies linked to aging [44, 45], and senolytic drugs such as dasatinib and quercetin (D + Q) have shown promise in enhancing physical function and muscle recovery in aged mice [17, 20, 46, 47]. We demonstrated similar benefits with p21 knockdown, linking senolytic effects to improved myoblast differentiation. Unlike past research that used p21 only as a senescence marker [48], our finding highlights its broader implications for muscle regeneration and function.

Our study has some limitations. While the C2-ceramide model is useful for studying aspects of sarcopenia, it does not fully replicate the complexity of aged muscle tissue. For example, C2-ceramide treatment followed by myotube differentiation did not reduce mitochondrial O₂ respiration or myotube number. In addition, determining whether the effectiveness of senolytics, such as D + Q, depends on p21 will be crucial for clarifying the role of p21 in muscle aging. Further validation in animal models with muscle tissue-specific or satellite cell-specific *Cdkn1a* regulation is required. Moreover, given roles of p21 beyond apoptosis—including anti-inflammatory effects [49, 50]—future research should explore potential off-target consequences of p21 inhibition. Finally, whether cells cleared by p21 inhibition exhibit characteristics of aging-related sarcopenia should be further confirmed in vivo.

Conclusions

Our study suggests that targeting p21 could be a promising therapeutic strategy for aging-related sarcopenia, by removing senescent cells and enhancing healthy myoblast regeneration. Nonetheless, further research in more comprehensive models is necessary to validate our findings and explore the full therapeutic potential of p21 inhibition.

Abbreviations

ADP	Adenosine diphosphate
ALT	Alanine aminotransferase
AST	Aspartate aminotransferase
CSA	Cross-sectional area
DEG	Differentially expressed gene
DM	Differentiation medium
ETC	Electron transport chain
FACS	Fluorescence-activated cell sorting
G3P	Glycerol-3-phosphate
GM	Growth medium
HDL	High-density lipoprotein
IL-6	Interleukin-6
LDL	Low-density lipoprotein
MHC	Myosin heavy chain
PBS	Phosphate buffered saline
PI	Propidium iodide
RIPA	Radioimmunoprecipitation assay
RT	Room temperature
SA- β -gal	Senescence-associated beta-galactosidase
SASP	Senescence-associated secretory phenotype
TNF- α	Tumor necrosis factor-alpha
WG	White gastrocnemius
WTS	Whole transcriptome sequencing

Supplementary Information

The online version contains supplementary material available at <https://doi.org/10.1186/s11658-025-00731-9>.

Supplementary Material 1.

Acknowledgements

The authors would like to thank Ms. Seung-Hee Kang for her elaborate illustration of the main and supplementary figures.

Author contributions

All authors have approved the final version of manuscript and have agreed to its publication. S.K. and B.G.: formal analysis, data curation, investigation, writing—original draft. K.E.K.M. and S.M.: methodology, investigation, and validation. S-H.J.: analysis and validation of whole transcriptome sequencing. C-Y.S., D-H.P., J.C., and E-J.C.: formal analysis, methodology, and writing—review and editing. H-B.K.: formal analysis, funding acquisition, and writing—review and editing. J-H.K.: conceptualization, supervision, and writing—review and editing. J-S.L.: conceptualization, funding acquisition, supervision, and writing—review and editing.

Funding

This work was supported by the Medical Research Center Program (NRF-2021R1A5A2031612) and Mid-Career Research Program (NRF-2018R1A2A3074577 and NRF-2023R1A2C1004370) through the National Research Foundation of Korea (NRF) funded by the Korean Government, and the NRF funded by the Ministry of Education (2022S1A5C2A03092407), Republic of Korea.

Data availability

The datasets from this study are available in online repositories, with details provided in the article or Supplementary Material. Supplementary information is available on the journal of "Cellular & Molecular Biology Letters" website.

Declarations

Ethics approval and consent to participate

Approval for all animal experiments was obtained from the Institutional Animal Care and Use Committee of Inha University (IACUC approval number, INHA-180807-587-5, 2020-01-29, Incheon, Korea). All of the experimental procedures involving animals were conducted in accordance with the Institutional Animal Care guidelines and the information that Local Ethics Committee acts on Animals (Scientific Procedures) Act 1986 in the UK and Directive 2010/63/EU in Europe.

Consent for publication

The manuscript has been approved by all the authors.

Competing interests

The authors declare that the research was conducted in the absence of any commercial or financial relationships that could be construed as a potential conflict of interest.

Author details

¹Department of Pharmacology, Inha University College of Medicine, 100, Inha-Ro, Michuhol-Gu, Incheon 22212, Republic of Korea. ²Research Center for Controlling Intercellular Communication, Inha University College of Medicine, Incheon 22212, Republic of Korea. ³Program in Biomedical Science and Engineering, Inha University, Incheon, South Korea. ⁴Department of Biochemistry, College of Medicine, The Catholic University of Korea, Seoul, Republic of Korea. ⁵Integrated Research Center for Genomic Polymorphism, College of Medicine, The Catholic University of Korea, Seoul, Republic of Korea. ⁶Department of Medical Sciences, Graduate School of The Catholic University of Korea, Seoul, Republic of Korea. ⁷Department of Kinesiology, Inha University, Incheon, Republic of Korea. ⁸College of Sport Science, Sungkunkwan University, Suwon, Republic of Korea. ⁹Department of Molecular Medicine, Inha University College of Medicine, 100, Inha-Ro, Michuhol-Gu, Incheon 22212, Republic of Korea.

Received: 28 October 2024 Accepted: 8 April 2025

Published online: 30 April 2025

References

1. Cruz-Jentoft AJ, Baeyens JP, Bauer JM, Boirie Y, Cederholm T, Landi F, et al. Sarcopenia: European consensus on definition and diagnosis: report of the European Working Group on Sarcopenia in Older People. *Age Ageing*. 2010;39(4):412–23.
2. Cruz-Jentoft AJ, Bahat G, Bauer J, Boirie Y, Bruyere O, Cederholm T, et al. Sarcopenia: revised European consensus on definition and diagnosis. *Age Ageing*. 2019;48(1):16–31.
3. Clegg A, Young J, Iliffe S, Rikkert MO, Rockwood K. Frailty in elderly people. *Lancet*. 2013;381(9868):752–62.
4. Vitale G, Salvioli S, Franceschi C. Oxidative stress and the ageing endocrine system. *Nat Rev Endocrinol*. 2013;9(4):228–40.
5. Lang T, Streeper T, Cawthon P, Baldwin K, Taaffe DR, Harris TB. Sarcopenia: etiology, clinical consequences, intervention, and assessment. *Osteoporos Int*. 2010;21(4):543–59.
6. Sousa-Victor P, Gutarra S, Garcia-Prat L, Rodriguez-Ubreva J, Ortet L, Ruiz-Bonilla V, et al. Geriatric muscle stem cells switch reversible quiescence into senescence. *Nature*. 2014;506(7488):316–21.
7. Andres V, Walsh K. Myogenin expression, cell cycle withdrawal, and phenotypic differentiation are temporally separable events that precede cell fusion upon myogenesis. *J Cell Biol*. 1996;132(4):657–66.
8. Guo K, Wang J, Andres V, Smith RC, Walsh K. MyoD-induced expression of p21 inhibits cyclin-dependent kinase activity upon myocyte terminal differentiation. *Mol Cell Biol*. 1995;15(7):3823–9.
9. Halevy O, Novitsch BG, Spicer DB, Skapek SX, Rhee J, Hannon GJ, et al. Correlation of terminal cell cycle arrest of skeletal muscle with induction of p21 by MyoD. *Science*. 1995;267(5200):1018–21.
10. Walsh K, Perlman H. Cell cycle exit upon myogenic differentiation. *Curr Opin Genet Dev*. 1997;7(5):597–602.
11. Pajalunga D, Crescenzi M. Restoring the cell cycle and proliferation competence in terminally differentiated skeletal muscle myotubes. *Cells*. 2021;10(10):2753.
12. Janicke RU, Sohn D, Essmann F, Schulze-Osthoff K. The multiple battles fought by anti-apoptotic p21. *Cell Cycle*. 2007;6(4):407–13.
13. Wang J, Walsh K. Resistance to apoptosis conferred by Cdk inhibitors during myocyte differentiation. *Science*. 1996;273(5273):359–61.
14. Englund DA, Jolliffe A, Aversa Z, Zhang X, Sturmlechner I, Sakamoto AE, et al. p21 induces a senescence program and skeletal muscle dysfunction. *Mol Metab*. 2023;67: 101652.
15. Perez K, Ciotlos S, McGirr J, Limbad C, Doi R, Nederveen JP, et al. Single nuclei profiling identifies cell specific markers of skeletal muscle aging, frailty, and senescence. *Aging (Albany NY)*. 2022;14(23):9393–422.
16. van Deursen JM. The role of senescent cells in ageing. *Nature*. 2014;509(7501):439–46.
17. Zhang X, Habiballa L, Aversa Z, Ng YE, Sakamoto AE, Englund DA, et al. Characterization of cellular senescence in aging skeletal muscle. *Nat Aging*. 2022;2(7):601–15.
18. Welle S, Brooks AI, Delehanty JM, Needler N, Bhatt K, Shah B, et al. Skeletal muscle gene expression profiles in 20–29 year old and 65–71 year old women. *Exp Gerontol*. 2004;39(3):369–77.
19. Passos JF, Nelson G, Wang C, Richter T, Simillion C, Proctor CJ, et al. Feedback between p21 and reactive oxygen production is necessary for cell senescence. *Mol Syst Biol*. 2010;6:347.
20. Huang Y, Wang B, Hassounah F, Price SR, Klein J, Mohamed TMA, et al. The impact of senescence on muscle wasting in chronic kidney disease. *J Cachexia Sarcopenia Muscle*. 2023;14(1):126–41.
21. Zhang X, Suda M, Zhu Y. Senolytics combat COVID-19 in aging. *Nat Aging*. 2023;3(7):762–3.
22. Heo JW, No MH, Cho J, Choi Y, Cho EJ, Park DH, et al. Moderate aerobic exercise training ameliorates impairment of mitochondrial function and dynamics in skeletal muscle of high-fat diet-induced obese mice. *FASEB J*. 2021;35(2): e21340.
23. No MH, Heo JW, Yoo SZ, Jo HS, Park DH, Kang JH, et al. Effects of aging on mitochondrial hydrogen peroxide emission and calcium retention capacity in rat heart. *J Exerc Rehabil*. 2018;14(6):920–6.
24. Bolger AM, Lohse M, Usadel B. Trimmomatic: a flexible trimmer for Illumina sequence data. *Bioinformatics*. 2014;30(15):2114–20.

25. Dobin A, Davis CA, Schlesinger F, Drenkow J, Zaleski C, Jha S, et al. STAR: ultrafast universal RNA-seq aligner. *Bioinformatics*. 2013;29(1):15–21.
26. Anders S, Pyl PT, Huber W. HTSeq—a Python framework to work with high-throughput sequencing data. *Bioinformatics*. 2015;31(2):166–9.
27. Varet H, Brillet-Gueguen L, Coppee JY, Dillies MA. SARTools: a DESeq2- and EdgeR-based R pipeline for comprehensive differential analysis of RNA-Seq data. *PLoS ONE*. 2016;11(6): e0157022.
28. Robinson MD, McCarthy DJ, Smyth GK. edgeR: a Bioconductor package for differential expression analysis of digital gene expression data. *Bioinformatics*. 2010;26(1):139–40.
29. Zhou Y, Zhou B, Pache L, Chang M, Khodabakhshi AH, Tanaseichuk O, et al. Metascape provides a biologist-oriented resource for the analysis of systems-level datasets. *Nat Commun*. 2019;10(1):1523.
30. Cho DE, Choi GM, Lee YS, Hong JP, Yeom M, Lee B, et al. Long-term administration of red ginseng non-saponin fraction rescues the loss of skeletal muscle mass and strength associated with aging in mice. *J Ginseng Res*. 2022;46(5):657–65.
31. Jadhav KS, Dungan CM, Williamson DL. Metformin limits ceramide-induced senescence in C2C12 myoblasts. *Mech Ageing Dev*. 2013;134(11–12):548–59.
32. Sligar J, DeBruin DA, Saner NJ, Philp AM, Philp A. The importance of mitochondrial quality control for maintaining skeletal muscle function across health span. *Am J Physiol Cell Physiol*. 2022;322(3):C461–7.
33. Endlicher R, Drahota Z, Stefkova K, Cervinkova Z, Kucera O. The mitochondrial permeability transition pore—current knowledge of its structure, function, and regulation, and optimized methods for evaluating its functional state. *Cells*. 2023;12(9):1273.
34. Ciciliot S, Rossi AC, Dyar KA, Blaauw B, Schiaffino S. Muscle type and fiber type specificity in muscle wasting. *Int J Biochem Cell Biol*. 2013;45(10):2191–9.
35. Bodine SC, Stitt TN, Gonzalez M, Kline WO, Stover GL, Bauerlein R, et al. Akt/mTOR pathway is a crucial regulator of skeletal muscle hypertrophy and can prevent muscle atrophy in vivo. *Nat Cell Biol*. 2001;3(11):1014–9.
36. Ogasawara R, Suginozaki T. Rapamycin-insensitive mechanistic target of rapamycin regulates basal and resistance exercise-induced muscle protein synthesis. *FASEB J*. 2018;14:fj201701422R.
37. Visser M, Pahor M, Taaffe DR, Goodpaster BH, Simonsick EM, Newman AB, et al. Relationship of interleukin-6 and tumor necrosis factor-alpha with muscle mass and muscle strength in elderly men and women: the Health ABC Study. *J Gerontol A Biol Sci Med Sci*. 2002;57(5):M326–32.
38. Chinzei N, Hayashi S, Ueha T, Fujishiro T, Kanzaki N, Hashimoto S, et al. P21 deficiency delays regeneration of skeletal muscular tissue. *PLoS ONE*. 2015;10(5): e0125765.
39. He Y, Xie W, Li H, Jin H, Zhang Y, Li Y. Cellular senescence in sarcopenia: possible mechanisms and therapeutic potential. *Front Cell Dev Biol*. 2021;9: 793088.
40. Biferi MG, Nicoletti C, Falcone G, Puggioni EMR, Passaro N, Mazzola A, et al. Proliferation of multiple cell types in the skeletal muscle tissue elicited by acute p21 suppression. *Mol Ther*. 2015;23(5):885–95.
41. Wang J, Song C, Cao X, Li H, Cai H, Ma Y, et al. MiR-208b regulates cell cycle and promotes skeletal muscle cell proliferation by targeting CDKN1A. *J Cell Physiol*. 2019;234(4):3720–9.
42. van Rooij E, Quiat D, Johnson BA, Sutherland LB, Qi X, Richardson JA, et al. A family of microRNAs encoded by myosin genes governs myosin expression and muscle performance. *Dev Cell*. 2009;17(5):662–73.
43. Birch J, Gil J. Senescence and the SASP: many therapeutic avenues. *Genes Dev*. 2020;34(23–24):1565–76.
44. Hernandez-Segura A, Nehme J, Demaria M. Hallmarks of cellular senescence. *Trends Cell Biol*. 2018;28(6):436–53.
45. Khosla S, Farr JN, Tchkonja T, Kirkland JL. The role of cellular senescence in ageing and endocrine disease. *Nat Rev Endocrinol*. 2020;16(5):263–75.
46. Dungan CM, Figueiredo VC, Wen Y, VonLehmden GL, Zdunek CJ, Thomas NT, et al. Senolytic treatment rescues blunted muscle hypertrophy in old mice. *Geroscience*. 2022;44(4):1925–40.
47. Dungan CM, Murach KA, Zdunek CJ, Tang ZJ, Nolt GL, Brightwell CR, et al. Deletion of SA beta-Gal+ cells using senolytics improves muscle regeneration in old mice. *Ageing Cell*. 2022;21(1): e13528.
48. Zhu Y, Tchkonja T, Pirtskhalava T, Gower AC, Ding H, Giorgadze N, et al. The Achilles' heel of senescent cells: from transcriptome to senolytic drugs. *Ageing Cell*. 2015;14(4):644–58.
49. Scatizzi JC, Mavers M, Hutcheson J, Young B, Shi B, Pope RM, et al. The CDK domain of p21 is a suppressor of IL-1beta-mediated inflammation in activated macrophages. *Eur J Immunol*. 2009;39(3):820–5.
50. Mavers M, Cuda CM, Misharin AV, Gierut AK, Agrawal H, Weber E, et al. Cyclin-dependent kinase inhibitor p21, via its C-terminal domain, is essential for resolution of murine inflammatory arthritis. *Arthritis Rheum*. 2012;64(1):141–52.

Publisher's Note

Springer Nature remains neutral with regard to jurisdictional claims in published maps and institutional affiliations.